

Two-Step Dual-Wavelength Flash Raman Mapping Method for Measuring Thermophysical Properties of Supported Two-Dimensional Nanomaterials

Aoran Fan ^a, Haidong Wang ^a, Weigang Ma ^a and Xing Zhang ^{a,*}

^a Key Laboratory for Thermal Science and Power Engineering of Ministry of Education,
Department of Engineering Mechanics, Tsinghua University, Beijing, 100084, China

***Contact:** Professor Xing Zhang, Key Laboratory for Thermal Science and Power Engineering of
Ministry of Education, Department of Engineering Mechanics, Tsinghua University, Beijing,
100084, China. Email: x-zhang@mail.tsinghua.edu.cn. Tel: 86-010-62772668.

ABSTRACT

To determine the thermophysical properties of supported two-dimensional nanomaterials, this paper developed a two-step dual-wavelength flash Raman mapping method. The thermal conductivity of the supported two-dimensional nanomaterial and the thermal contact conductance between the sample and the substrate can be determined by steady-state step. And then the thermal diffusivity of the sample can be characterized by the transient step. Two models are also proposed in this paper. When the substrate temperature rises obviously, a full model considered the substrate temperature distribution is used to decouple the thermal diffusivity, thermal conductivity, and the thermal contact conductance. When the maximum substrate temperature rise is less than 20% of the maximum sample temperature rise, the temperature distribution and variation of the substrate is assumed proportionate to the sample, and then a simplified model can be used to analyse the

thermal diffusivity and the other parameters. For the thermal diffusivity, the system error caused by simplifying assumptions is less than 1%, when a dimensionless parameter related to the thermal contact conductance and the thermal conductivity less than 1 and the maximum temperature rise of the substrate less than 15% of that of the supported sample.

INTRODUCTION

Due to the superconductivity [1, 2], pyroelectricity [3], and other novel properties [4, 5], the two-dimensional nanomaterials have been the focus of recent research and could be the basement of the next-generation electronic productions [6-8]. Thus, the characterization of the thermophysical properties of nanomaterials is of great importance. However, in practical electronic devices, nanomaterials are usually supported on a substrate, and the interfacial electron or phonon scattering will also influence the thermophysical properties of supported nanomaterials compared with that of suspended nanomaterials [9-12]. Therefore, the in-situ measurement of the thermophysical properties of the supported nanomaterial is essential.

There are two significant methods on the measurement of the thermophysical properties of supported two-dimensional nanomaterials: the contact method [13-18] and the non-contact method [11, 12, 19-21]. For the contact method, researchers have used it to determine the thermal conductivity of supported graphene, and measured the thermal contact conductance between the graphene and the silicon dioxide substrate. However, the influence of electrical/thermal contact

resistance between the electrode and the sample is hard to be eliminated, and the temperature rise of the substrate cannot be measured directly, which would increase the measurement uncertainty.

For non-contact method, the thermo-domain thermal reflection (TDTR) method [19-21] has been widely used to determine the thermophysical properties of the supported nanofilm, especially metal nanofilm. However, in the TDTR method, the metal sensor on the sample surface should be more than 10 nm, which makes it not an ideal method for ultrathin nanofilm. As another non-contact method, the Raman method seems as the most promising method to study supported nanomaterial. It can determine the temperature variation of the monatomic film directly, such as graphene, and can measure the temperature variation of the substrate simultaneously. However, for the supported nanofilm, the laser absorptivity is hard to measure, which will significantly affect the measurement accuracy of the most used steady-state Raman method [4, 11, 22]. Some methods [23, 24] have been developed to directly measure the optical absorptivity by combining electrical and optical measurement, however, the methods are still limited by complex nanofabrication.

The transient Raman method [12, 25-31] can eliminate the laser absorption influence by normalization, and this method has been developed to determine the thermal diffusivity of the suspended one-dimensional, two-dimensional nanomaterials, the supported van der Waals heterostructures, and the thermal contact resistance between two carbon fibers. However, due to the limitation of temporal resolution and spatial resolution of previous measurement methods, the measurement sensitivity of the supported two-dimensional nanomaterial is still not satisfactory, and

the influence of multi thermal parameters have not decoupled directly in the model yet, which will also increase the uncertainty.

In our recent work, a transient dual-wavelength flash Raman (DFR) mapping method [32-35] with 100 ps temporal resolution and 50 nm spatial resolution was proposed, and was further developed to determine the thermal diffusivity of suspended one-dimensional [35], two-dimensional [33], and anisotropic nanomaterials [34]. However, this method has not been applied to supported two-dimensional nanomaterials yet. Because for suspended nanomaterials, the thermal diffusivity is the only one effect factor of the non-dimensional transient heat conduction proceeding. But for the supported nanomaterials, the transient heat conduction proceeding can be also influenced by the thermal conductance between the sample and the substrate. More information is needed for the thermal diffusivity measurement of the supported sample.

Therefore, based on the DFR mapping method, this paper presents a two-step DFR mapping method which further considered the steady-state heat conduction proceeding. The heating laser and the probing laser have different wavelength to make the Raman spectra excited by probing laser can be distinguished. In practice, the wavelength of the probing laser is always longer than the heating laser. In the steady-state step, by changing the center distance between the continuous heating laser spot and the continuous probing laser spot, the temperature distribution of the sample and the substrate can be measured by their Raman peak shift, and then the thermal conductivity of the supported sample and thermal contact conductance between the sample and the substrate can be

analyzed. Through the normalization approach to analyze the temperature difference between the supported sample and the substrate, this steady-state measurement can directly characterize the influence of laser absorptivity, which is significantly distinguished from the previous steady-state Raman methods [4, 11, 22]. In the transient step, the heating laser and probing laser are pulsed, and then the time delay between the two pulsed lasers is changed to determine the temperature variation of the sample and the substrate, and then the thermal diffusivity of the sample can be determined. Therefore, through this method, the influence of multi thermal parameters can be decoupled with high sensitivity.

Meanwhile, due to the small thermal capacity of nanofilm, the temperature of the substrate is always obviously smaller than it of the sample. When the absolute uncertainty is certain, the relative temperature measurement uncertainty of the substrate would be significantly larger than it of the sample, which makes the measurement of the substrate temperature distribution hard and inaccurate. In the previous methods, the small temperature rise of the substrate is always ignored [11-13]. This paper provides a new simplified model which just needs to measure the maximum temperature rise of the substrate. The error analysis shows that, when the substrate temperature rise is less than 15% of the sample temperature rise and a dimensionless parameter CC less than 1, the system error of the thermal diffusivity caused by simplifying assumptions is less than 1%, while the system error caused by ignoring substrate temperature rise can reach to 5.6% in this case. The simplified model can greatly decrease the system error compared with the model ignored substrate

temperature rise. And compared with the full model, this model can simplify the measurement and enhance the feasibility of the method.

FULL MODEL AND SENSITIVITY ANALYSIS

Physical model and solution

As shown in Figure 1, a periodic pulse Gaussian laser beam was used to heat the two-dimensional nanomaterial sample and the substrate, and another laser pulse with different wavelength and negligible heat effect is used as a probe to simultaneously measure the temperature variations of the sample and the substrate. The heating pulse width is t_h and the heating pulse interval, t_c , is long enough for the sample temperature to recover to the ambient temperature. When the wavelength of the heating laser differs from that of the probing laser, the Raman spectra excited by the heating pulse and the probing pulse can be distinguished, and the sample temperature variations can be determined from the Raman peak shifts excited by the probing pulse. The temperature variations are the average temperature variations during the pulse width of the probing pulse, t_p , with the temperature variations during the heating and cooling periods measured by changing the time delay between the heating and probing pulse, t_d . In addition, the position of the probing laser spot can be moved by a scanning mirror. With a fixed heating laser spot, the temperature variation at arbitrary time delay and the optional position can be measured. When the thermophysical properties of the substrate are known, through the steady-state measurement and the transient measurement, the contact thermal conductance g between the substrate and the

nanomaterial, the thermal diffusivity α_n , and thermal conductivity λ_n of the supported two-dimensional nanomaterial can be determined.

There are two steps to this method. The first one is the steady-state step. By changing the centre distance between the continuous heating laser spot and the continuous probing laser spot, the temperature distribution of the sample and the substrate can be measured, and then the thermal conductivity and thermal contact conductance can be analysed. The interfacial heat flux is more than 5 orders larger than the heat loss of radiation and convection [11]. Thus, in a vacuum, the heat loss of the environment can be neglected, and the heat conduction in steady-state can be expressed as:

$$\frac{\partial^2 \theta_n^{st}(r)}{\partial r^2} + \frac{1}{r} \frac{\partial \theta_n^{st}(r)}{\partial r} + \frac{\eta_n q_h}{\lambda_n \delta} \exp(-r^2 / r_h^2) - \frac{g}{\lambda_n \delta} (\theta_n^{st}(r) - \theta_{sub}^{st}(r, 0)) = 0 \quad (1)$$

$$\begin{aligned} \frac{\partial^2 \theta_{sub}^{st}(r, z, t)}{\partial r^2} + \frac{1}{r} \frac{\partial \theta_{sub}^{st}(r, z, t)}{\partial r} + \frac{\partial^2 \theta_{sub}^{st}(r, z, t)}{\partial z^2} &= 0 \\ -\lambda_{sub} \frac{\partial \theta_{sub}^{st}(r, 0)}{\partial z} &= g \times (\theta_n^{st}(r) - \theta_{sub}^{st}(r, 0)) + \eta_{sub} q_h \exp(-r^2 / r_h^2) \end{aligned} \quad (2)$$

where $\theta_n^{st}(r)$ is the temperature rise of the supported two-dimensional nanomaterial sample at radius r in steady state, $\theta_{sub}^{st}(r, z)$ is the temperature rise of the substrate at radial position r and axial position z in steady state, g is the contact thermal conductance between the sample and the substrate, η_n , λ_n and δ are respectively the effective laser absorptivity, the thermal conductivity and the thickness of the sample, η_{sub} and λ_{sub} are respectively the effective laser absorptivity and the thermal conductivity of the substrate, q_h is the laser power density of the heating pulse at the beam

center, and r_h is the laser spot radius of the heating pulse where the power density attenuates to q_h/e .

Due to the interaction effect between the supported nanomaterial and the substrate, the decoupling of the parameters will be complicated. To simply the parameter decoupling, the temperature difference between the supported two-dimensional nanomaterial sample and the substrate is considered as an independent variable. Then the heat conduction of the supported sample in steady-state can be expressed as:

$$\frac{\partial^2 \theta_n^{st}(r)}{\partial r^2} + \frac{1}{r} \frac{\partial \theta_n^{st}(r)}{\partial r} + \frac{\eta_n q_h}{\lambda_n \delta} \exp(-r^2 / r_h^2) - \frac{g}{\lambda_n \delta} f^{st}(r) = 0 \quad (3)$$

where $f^{st}(r) = \theta_n^{st}(r) - \theta_{sub}^{st}(r, 0)$ is the temperature difference between the supported nanomaterial and the substrate in steady-state. By applying Hankel transform, $f^{st}(r)$ can be described as:

$$f^{st}(r) = \frac{\lambda_n \delta}{g} \left(\frac{\eta_n q_h \exp(-r^2 / r_h^2)}{\delta} - \sum_{m=1}^{\infty} \mu_m^2 \theta_n^{st,*}(\mu_m) K_0(\mu_m, r) \right) \quad (4)$$

where the kernel $K_0(\mu_m, r)$ is

$$K_0(\mu_m, r) = \frac{\sqrt{2}}{R} \frac{J_0(\mu_m r)}{J_1(\mu_m R)} \quad (R \rightarrow \infty) \quad (5)$$

where J_0 and J_1 are the zero-order and first-order Bessel functions of the first kind. The characteristic values, μ_m , are $\mu_m = \beta_m / R$, β_m are the positive roots of the first-order Bessel functions, R is the dimensionless characteristic length. And the $\theta_n^{st,*}(\mu_m)$ is the Hankel transformation of $\theta_n^{st}(r)$

$$\theta_n^{st,*}(\mu_m) = \int_0^\infty \theta_n^{st}(r) K_0(\mu_m, r) r dr \quad (6)$$

Therefore, the parameter η_n/λ_n can be determined by the relationship between the normalized temperature difference, $f^{st}(r)/f^{st}(0)$, and the temperature distribution of the sample, $\theta_n^{st}(r)$, then the parameter λ_n/g can be then determined with the measured η_n/λ_n .

Correspondingly, the heat conduction of the substrate in steady state can be expressed as:

$$\begin{aligned} \frac{\partial^2 \theta_{sub}^{st}(r, z)}{\partial r^2} + \frac{1}{r} \frac{\partial \theta_{sub}^{st}(r, z)}{\partial r} + \frac{\partial^2 \theta_{sub}^{st}(r, z)}{\partial z^2} &= 0 \\ -\lambda_{sub} \frac{\partial \theta_{sub}^{st}(r, 0)}{\partial z} &= g \times f^{st}(r) + \eta_{sub} q_h \exp(-r^2 / r_h^2) \end{aligned} \quad (7)$$

where $\theta_{sub}^{st}(r, z)$ is the temperature distributions of the substrate in steady-state. By applying Hankel transform, $f^{st}(r)$ can be described as a function of the temperature of the substrate surface:

$$f^{st}(r) = \frac{\lambda_{sub}}{g} \left(\sum_{m=1}^{\infty} \mu_m \theta_{sub}^{st,*}(\mu_m, 0) K_0(\mu_m, r) - \frac{\eta_{sub}}{\lambda_{sub}} q_h \exp(-r^2 / r_h^2) \right) \quad (8)$$

where $\theta_{sub}^{st,*}(\mu_m, 0)$ is the Hankel transformation of $\theta_{sub}^{st}(r, 0)$,

$$\theta_{sub}^{st,*}(\mu_m, 0) = \int_0^\infty \theta_{sub}^{st}(r, 0) K_0(\mu_m, r) r dr \quad (9)$$

Therefore, the parameter η_{sub}/λ_{sub} can be determined by the relationship between the normalized temperature difference, $f^{st}(r)/f^{st}(0)$, and the temperature distribution of the substrate surface, $\theta_{sub}^{st}(r, 0)$, and then λ_{sub}/g can be then determined with the measured η_{sub}/λ_{sub} .

With the known thermal conductivity of the substrate, λ_{sub} , the contact thermal conductance g can be characterized. And then the thermal conductivity, λ_n , and laser absorptivity, η_n , of the supported nanomaterial sample can be determined with the measured λ_n/g and η_n/λ_n .

The second step of this method is the transient step, the heating laser and probing laser are pulsed, and then the time delay between the two pulsed lasers are changed to determine the temperature variation of the sample and the substrate, and then the thermal diffusivity of the sample can be determined. With the temperature difference between the sample and the substrate surface denoted as $f(r,t) = \theta_n(r,t) - \theta_{sub}(r,0,t)$, the heat conduction of the supported two-dimensional nanomaterial sample can be expressed as Eq. (10).

$$\frac{\partial^2 \theta_n(r,t)}{\partial r^2} + \frac{1}{r} \frac{\partial \theta_n(r,t)}{\partial r} + \frac{\Phi_n(r,t)}{\delta} = \frac{1}{\alpha_n} \frac{\partial \theta_n(r,t)}{\partial t}$$

$$\Phi_n(r,t) = \begin{cases} \frac{\eta_n q_h}{\lambda_n} \exp(-r^2 / r_h^2) - \frac{g}{\lambda_n} \times f(r,t) & (t \leq t_h) \\ -\frac{g}{\lambda_n} \times f(r,t) & (t > t_h) \end{cases} \quad (10)$$

where $\theta_n(r, t)$ is the temperature rise of the supported two-dimensional nanomaterial sample at radius r and time t , $\theta_{sub}(r, z, t)$ is the temperature rise of the substrate at position (r, z) and time t , α_n is the thermal diffusivities of the sample.

The initial temperature rise of the supported nanomaterial is 0; and the boundary conditions at $r = 0$ are given by the symmetry conditions as

$$\frac{\partial \theta_n(0,t)}{\partial r} = 0 \quad (11)$$

The boundary conditions at infinity are

$$\theta_n(\infty,t) = 0 \quad (12)$$

The analytical solution for the temperature rises of the supported two-dimensional nanomaterial sample and the substrate are obtained by successively applying Hankel and Laplace transforms

$$\theta_n(r, t) = \sum_{m=1}^{\infty} \theta_n^*(\mu_m, t) K_0(\mu_m, r) \quad (13)$$

where the $\theta_n^*(\mu_m, t)$ is the Hankel transformation of the temperature variation of the supported nanomaterial, which is obtained from the inverse Laplace transformation,

$$\theta_n^*(\mu_m, t) = \begin{cases} \left[\begin{array}{l} \frac{\eta_n q_h e^*(\mu_m)}{\mu_m^2 \lambda_n \delta} (1 - \exp(-\alpha_n \mu_m^2 t)) \\ - \frac{\alpha_n g}{\lambda_n \delta} \int_0^t f^*(\mu_m, \tau) \exp(-\alpha_n \mu_m^2 (t - \tau)) d\tau \end{array} \right] & (t \leq t_h) \\ \left[\begin{array}{l} \theta_n^*(\mu_m, t_h) \exp(-\alpha_n \mu_m^2 t) \\ - \frac{\alpha_n g}{\lambda_n \delta} \int_0^t f^*(\mu_m, \tau) \exp(-\alpha_n \mu_m^2 (t - \tau)) d\tau \end{array} \right] & (t > t_h) \end{cases} \quad (14)$$

where $e^*(\mu_m)$ and $f^*(\mu_m, t)$ are the Hankel transformation of $\exp(-r^2 / r_h^2)$ and $f(r, t)$, respectively.

$$e^*(\mu_m) = \int_0^R \exp(-r^2 / r_h^2) K_0(\mu_m, r) r dr \quad (15)$$

$$f^*(\mu_m, t) = \int_0^R f(r, t) K_0(\mu_m, r) r dr \quad (16)$$

According to the above solution, with the measured η_n / λ_n and g / λ_n , the thermal diffusivity of the sample, α_n , can be determined.

Sensitivity analysis of full model

Several cases were simulated to analyse the sensitivity of the two-step DFR mapping method. Figure 2 shows the sensitivity of the temperature difference $f^{st}(r)$ in a steady state with a certain temperature distribution of substrate surface $\theta_{sub}^{st}(r,0)$ calculated by a silicon substrate with 35 K temperature rise. For typical η_{sub}/λ_{sub} and λ_{sub}/g with $\pm 10\%$ variations, when the laser spot radius of the heating laser r_h is 259 nm, the maximum sensitivities to the various η_{sub}/λ_{sub} from 5×10^{-7} m K/W to 2×10^{-6} m K/W are respectively 3.2%, 5.3% and 6.1%, while the maximum sensitivities to the various λ_{sub}/g is 10% when $r=0$.

Figure 3 shows the sensitivity of the temperature difference $f^{st}(r)$ in a steady state with a certain temperature distribution of the supported sample $\theta_n^{st}(r)$ calculated by a supported graphene with 50 K temperature rise. As shown in Figure 4(a), the normalized temperature difference is more sensitive to small parameter η_n/λ_n . When $\eta_n/\lambda_n = 5 \times 10^{-6}$ m K/W, with η_n/λ_n changes $\pm 10\%$, the normalized temperature variation at $r = 500$ nm can reach to -0.10/+0.26. While the maximum sensitivities to the various λ_n/g is also 10% when $r=0$.

With the determined thermal contact conductance g and thermal conductivity λ_n , the thermal diffusivity can be determined by the normalized temperature rise curves of the supported sample as shown in Figure 4. In this case, the temperature difference $f(r,t)$ is assumed as 0.01 of the temperature rise of the corresponding suspended sample. The temperature variation curves are more sensitive in cooling proceeding. When thermal diffusivity changes $\pm 10\%$, the maximum

normalized temperature variation to the various α_n from $1 \times 10^{-3} \text{ m}^2/\text{s}$ to $1 \times 10^{-5} \text{ m}^2/\text{s}$ are respectively ± 0.024 , ± 0.019 and ± 0.023 . Therefore, when the measurement uncertainty of normalized temperature is 0.01, the measurement uncertainty of the thermal diffusivity caused by transient temperature measurement is about $\pm 5\%$.

SIMPLIFIED MODEL AND FEASIBILITY ANALYSIS

Simplified model for supported two-dimensional nanomaterials

In practice, the temperature rise of the substrate is always significantly lower than it of the supported two-dimensional nanomaterial, and the temperature distribution of the substrate would be hard to determine. Fortunately, in this case, the influence of the substrate temperature distribution on the supported sample would be also decreased. Thus, the temperature distribution of the substrate can be assumed as $\theta_{sub}^{st}(r, 0) = \delta T_{ste} \times \theta_n^{st}(r)$, where $\delta T_{ste} = \theta_{sub}^{st}(0, 0) / \theta_n^{st}(0)$. With the nondimensionalized techniques, the heat conduction equation in steady-state can be written as:

$$\frac{d^2 T_{ste}(x)}{dx^2} + \frac{1}{x} \frac{dT_{ste}(x)}{dx} - CC(1 - \delta T_{ste}) \times T_{ste}(x) + \exp(-x^2) = 0 \quad (17)$$

where $x = r/r_h$ is the dimensionless coordinate with the characteristic length, r_h , $T_{ste} = \theta_n^{st} / \theta_0$ is the dimensionless temperature rises of the supported sample with $\theta_0 = \eta_n q h r_h^2 / \lambda_n \delta$ as the characteristic temperature rise, and $CC = g r_h^2 / \lambda_n \delta$ is a dimensionless number which influence the heat transfer between the supported sample and the substrate. The analytical solution of the sample temperature rise T_{st} can be obtained by applying Hankel transform, and which is given by

$$T_{ste}(x) = \sum_{n=1}^{\infty} \frac{E^*(\mu_m) K_0(\mu_m, x)}{\mu_m^2 + CC_{ste}} \quad (18)$$

where $E^*(\mu_m) = \int_0^R \exp(-x^2) K_0(\mu_m, x) x dx$, and $CC_{ste} = CC \times (1 - \delta T_{ste})$.

Analogously, in transient measurement, the temperature variation of the substrate can be assumed as $\theta_{sub}(r, 0, t) = \delta T \times \theta_n(r, t)$, where $\delta T = \theta_{sub}(0, 0, t_h) / \theta_n(0, t_h)$. Using the same characteristic length r_h , the same characteristic temperature θ_0 , and a characteristic time t_0 , the nondimensionalized transient heat conduction of the sample can be described as:

$$\frac{\partial^2 T(x, \tau)}{\partial x^2} + \frac{1}{x} \frac{\partial T(x, \tau)}{\partial x} - CC(1 - \delta T) \times T(x, \tau) + \Phi(x, \tau) = \frac{1}{Fo} \frac{\partial T(x, \tau)}{\partial \tau} \quad (19)$$

$$\Phi(r, t) = \begin{cases} \exp(-x^2) & (\tau \leq \tau_h) \\ 0 & (\tau > \tau_h) \end{cases}$$

where $T = \theta_n / \theta_0$ is the transient dimensionless temperature rises of the supported sample with θ_0 as the characteristic temperature rise, $\tau = t/t_0$, $\tau_h = t_h/t_0$, and $Fo = \alpha_n t_0 / r_h^2$.

By Hankel transform, the analytical solution of the sample temperature variation can be obtained as:

$$T(x, \tau) = \sum_{m=1}^{\infty} T^*(\mu_m, \tau) K_0(\mu_m, x) \quad (20)$$

where $T^*(\mu_m, \tau)$ is expressed as Eq. (21) with $CC_e = CC(1 - \delta T)$.

$$T^*(\mu_m, \tau) = \begin{cases} \frac{E^*(\mu_m)}{\mu_m^2 + CC_e} \left[1 - \exp(-Fo(\mu_m^2 + CC_e)\tau) \right] & (\tau \leq \tau_h) \\ T^*(\mu_m, \tau_h) \exp(-Fo(\mu_m^2 + CC_e)(\tau - \tau_h)) & (\tau > \tau_h) \end{cases} \quad (21)$$

Therefore, during the steady-state measurement, with the measured normalization temperature distribution of the supported sample and the steady-state temperature ratio δT_{st} , the dimensionless

number CC can be determined by Eq. (18). With the measured CC and the transient temperature ratio δT , the Fourier number $Fo = \alpha_n t_0 / r_h^2$ can be characterized by normalized temperature variation of the supported sample during heating and cooling proceeding. Due to the t_0 is a parameter chosen by the researcher to ensure the equation convergence, and r_h is the laser radius determined by the heating laser wavelength and the numerical aperture of the optical, thus the thermal diffusivity α_n can be determined. With known density ρ and specific heat c_p , the thermal conductivity $\lambda_n = \alpha_n \rho c_p$ can be further characterized. With known sample thickness δ , the thermal contact conductance g can be calculated by $g = CC \lambda_n \delta / r_h^2$.

Sensitivity analysis of simplified model

Figure 5(a) shows the normalized temperature distribution Θ^{st} in steady-state with various parameter CC_{ste} , and Figure 5(b) shows the measurement sensitivity $\Delta\Theta^{st}$, which is defined as $\Delta\Theta^{st} = \left| \Theta^{st}(CC_{ste} + 20\%) - \Theta^{st}(CC_{ste} - 20\%) \right|$. It can be observed that the sample with the larger parameter CC_{ste} has a higher maximum sensitivity, while the sample with the smaller parameter CC_{ste} has a larger sensitive region.

When choose $t_0 = l^2 / \alpha_n$, l is the characteristic length, the Fourier number Fo will always be 1 for any sample. Figure 6 shows the transient normalized temperature variations Θ during transient measurement at different positions and with different parameter CC_e , where x_{h-p} describes the dimensionless length between the centers of the heating laser spot and the probing laser spot. It can be observed that for smaller CC_e , the temperature variation curves would have higher

sensitivity with a larger x_{h-p} , while the sensitivity difference would be no noticeable when CC_e increase.

Feasibility analysis of the simplified model

The feasibility of the assumption used in the simplified model should be analysed. Figure 7 shows the system error of $CC = gr_h^2/\lambda_n\delta$ caused by the simplifying assumption with various δT_{ste} and CC . It can be observed that when δT_{ste} less than 0.05, the system error of CC caused by simplifying assumption will less than 0.1%, while the system error caused by ignoring the substrate temperature rise will be almost 5%. The simplified model significantly decreases the system error compared with the model ignored the substrate temperature rise. For most measurement cases, the temperature ratio δT_{ste} will less than 0.15 and CC less than 1, and the system error of CC no more than 1.1%, which shows the simplified model will be feasible for most steady-state measurements.

Figure 8 shows the system error of α_n caused by the simplifying assumption with various δT and CC . With CC increases, the thermal contact conductance g increases, and the influence of substrate temperature variation on the sample temperature variation increases and makes the system error increase. Meanwhile, with g increases, the temperature variation curves of the sample become more like the temperature variation curves of the substrate and which makes the system error decreases. The two opposite factors make an extremum of the system error in the thermal diffusivity α_n measurement. It can be observed that when δT less than 0.15 and CC less than 1, the system error of CC caused by simplifying assumption will less than 1%. Correspondingly, as

shown in Figure 9, with the same δT and CC , the system error caused by ignoring substrate temperature rise can reach to 5.6%. This further shows the advantages of the simplified model compared with the model ignored substrate temperature rise.

CONCLUSIONS

This paper presents a two-step DFR method for determining the thermal diffusivity, thermal conductivity, and contact thermal conductance of supported two-dimensional materials. In the first steady-state step, a continuous heating laser is used to heat the sample and the substrate to steady-state, another continuous probe laser, with a different wavelength and the neglectable heating effect, is used to determine the temperature distributions of the sample and the substrate. The thermal conductivity and the contact thermal conductance can be extracted by fitting the normalized temperature distribution of the sample and the substrate. In the second transient step, the pulsed heating laser is used to heat the sample and the substrate, and the probing pulse laser with various time delay is used to measure the temperature rises of the sample and the surface of the substrate simultaneously, then the thermal diffusivities α_n can be determined.

Furthermore, two models are proposed in this paper. When the substrate temperature rises obviously, a full model considered the substrate temperature distribution is used to decouple the thermal diffusivity, thermal conductivity, and the thermal contact conductance. When the measurement uncertainty of normalized temperature is 0.01, with a full model the measurement uncertainty of the various thermal diffusivity caused by transient temperature measurement is about

$\pm 5\%$. When the maximum substrate temperature rise is less than 20% of the maximum sample temperature rise, the temperature distribution and variation of the substrate is assumed proportionate to the sample, and then a simplified model can be used to analyze the thermal diffusivity and the other parameters. For the thermal diffusivity, the system error caused by simplifying assumptions is less than 1% when a dimensionless parameter CC less than 1 and the maximum temperature rise of the substrate less than 15% of that of the supported sample, while, with the same substrate temperature rise and CC , the system error caused by ignoring substrate temperature rise can reach to 5.6%. The simplified model can greatly decrease the system error compared with the model ignored substrate temperature rise. And compared with the full model, this model can simplify the measurement and enhance the feasibility of the method.

NOMENCLATURE

c_p specific heat [$\text{J kg}^{-1} \text{K}^{-1}$]

CC dimensionless parameter $CC = gr_h^2/\lambda_n\delta$

DFR dual-wavelength flash Raman

Fo Fourier number

f temperature difference between the supported nanomaterial and substrate [K]

g thermal contact conductance [$\text{W m}^{-2} \text{K}^{-1}$]

J_0 zero-order Bessel function

J_1	first-order Bessel function
K	kernel function
l	characteristic length [m]
q	laser power density [W m^{-2}]
r	cylindrical coordinate [m]
R	dimensionless characteristic length
r_{h-p}	distance between the centers of heating laser spot and probing laser spot [m]
t	time [s]
T	normalized temperature rise
t_c	heating pulse interval [s]
t_d	time delay between the heating and probing pulse [s]
TDTR	thermo-domain thermal reflection
t_h	heating pulse width [s]
t_p	probing pulse width [s]
x	dimensionless coordinate with characteristic length
x_{h-p}	dimensionless distance between the centers of heating laser spot and probing laser spot
z	cylindrical coordinate [m]

Greek symbols

α	thermal diffusivity [$\text{m}^2 \text{s}^{-1}$]
β_m	positive roots of the first-order Bessel function
δ	thickness of two-dimensional nanomaterial [m]
η	laser absorptivity
λ	thermal conductivity [$\text{W m}^{-1} \text{K}^{-1}$]
θ	temperature rise [K]
μ_m	the ratio of characteristic roots of Bessel function to R
τ	characteristic time
τ_d	dimensionless time delay between the heating and probing pulse
τ_h	dimensionless heating pulse width
ρ	density [kg m^{-3}]
Θ	normalized temperature distribution

Subscripts

e	effective value of transient state
h	heating laser
n	two-dimensional nanomaterial
p	probing laser
ste	effective value of steady state

sub substrate

0 characteristic value

Superscripts

st steady state

* Hankel transformation

ACKNOWLEDGMENTS

This work was supported by the National Natural Science Foundation of China (Grant Nos. 51827807 and 51636002).

REFERENCES

- [1] D. M. Guzman, H. M. Alyahyaei, and R. A. Jishi, “Superconductivity in graphene-lithium”, *2D Mater.*, vol. 1, no. 2, article no. 021005 (16 pages), Sept. 2014. DOI:10.1088/2053-1583/1/2/021005.
- [2] Y. Cao *et al.*, “Unconventional superconductivity in magic-angle graphene superlattices”, *Nature*, vol. 556, pp. 43-50, Mar. 2018. DOI:10.1038/nature26160.
- [3] Y. C. Hu, W. L. Hsu, Y. T. Wang, C. T. Ho, and P. Z. Chang, “Enhance the Pyroelectricity of Polyvinylidene Fluoride by Graphene-Oxide Doping”, *Sensors-Basel*. vol. 14, no. 4, pp.6877-6890, Apr. 2014. DOI:10.3390/s140406877.

- [4] A. A. Balandin *et al.*, “Superior thermal conductivity of single-layer graphene”, *Nano Lett.*, vol. 8, no. 3, pp. 902-907, Mar. 2008. DOI:10.1021/nl0731872.
- [5] G. Narendran, N. Gnanasekaran, and D. A. Perumal, “Experimental Investigation on Heat Spreader Integrated Microchannel Using Graphene Oxide Nanofluid”, *Heat Transfer Eng.*, vol. 41, no. 14, pp. 1252-1274, Aug. 2019. DOI:10.1080/01457632.2019.1637136.
- [6] J. L. Smoyer and P. M. Norris, “Brief Historical Perspective in Thermal Management and the Shift Toward Management at the Nanoscale”, *Heat Transfer Eng.*, vol. 40, no. 3-4, pp. 269-282, Feb. 2019. DOI:10.1080/01457632.2018.1426265.
- [7] G. Chen, “Nanoscale heat transfer and nanostructured thermoelectrics”, *IEEE T. Comp. Pack. Man.*, vol. 29, no. 2, pp. 238-246, May 2006. DOI:10.1109/TCAPT.2006.875895.
- [8] D. G. Cahill *et al.*, “Nanoscale thermal transport. II. 2003–2012”, *Appl. Phys. Rev.*, vol. 1, no. 1, article no. 011305 (45 pages), Jan. 2014. DOI:10.1063/1.4832615.
- [9] Z. Y. Ong, E. Pop, and J. Shiomi, “Reduction of phonon lifetimes and thermal conductivity of a carbon nanotube on amorphous silica”, *Phys. Rev. B*, vol. 84, no. 16, article no. 165418 (25 pages), Oct. 2011. DOI:10.1103/PhysRevB.84.165418.
- [10] Z. Wang *et al.*, “Thermal transport in suspended and supported few-layer graphene”, *Nano Lett.*, vol. 11, no. 1, pp. 113-118, Jan. 2011. DOI:10.1021/nl102923q.
- [11] W. W. Cai *et al.*, “Thermal Transport in Suspended and Supported Monolayer Graphene Grown by Chemical Vapor Deposition”, *Nano Lett.*, vol. 10, no. 5, pp. 1645-1651, May 2010. DOI:

10.1021/nl9041966.

[12] Q. Y. Li *et al.*, “Measurement of specific heat and thermal conductivity of supported and suspended graphene by a comprehensive Raman optothermal method”, *Nanoscale*, vol. 9, no. 30, pp. 10784-10793, Aug. 2017. DOI: 10.1039/c7nr01695f.

[13] J. H. Seol *et al.*, “Two-dimensional phonon transport in supported graphene”, *Science*, vol. 328, no. 5975, pp. 213-216, Apr. 2010. DOI:10.1126/science.1184014.

[14] G. Zhou and D. Wang, “Few-quintuple Bi₂Te₃ nanofilms as potential thermoelectric materials”, *Sci. Rep.*, vol. 5, article no. 8099 (6 pages), Jan. 2015. DOI: 10.1038/srep08099.

[15] Z. Chen, W. Jang, W. Bao, C. N. Lau, and C. Dames, “Thermal contact resistance between graphene and silicon dioxide”, *Appl. Phys. Lett.*, vol. 95, no. 16, article no. 161910 (3 pages), Spet. 2009. DOI:10.1063/1.3245315.

[16] Q. Y. Li *et al.*, “Enhanced thermoelectric performance of as-grown suspended graphene nanoribbons”, *ACS nano*, vol. 13, no. 8, pp. 9182-9189, Aug. 2019. DOI: 10.1021/acsnano.9b03521.

[17] M. Narasaki *et al.*, “Modification of thermal transport in an individual carbon nanofiber by focused ion beam irradiation”, *Carbon*, vol. 153, pp. 539-544, Nov. 2019. DOI: 10.1016/j.carbon.2019.07.056.

- [18] Q. Y. Li *et al.*, “Temperature dependent thermal conductivity of a suspended submicron graphene ribbon”, *J. Appl. Phys.*, vol. 117, no. 6, article no. 065102 (6 pages), Feb. 2015. DOI: 10.1063/1.4907699.
- [19] N. Taketoshi, T. Baba, and A. Ono, “Development of a thermal diffusivity measurement system for metal thin films using a picosecond thermoreflectance technique”, *Meas. Sci. Technol.*, vol. 12, no. 12, pp. 2064-2073, Nov. 2001. DOI:10.1088/0957-0233 /12/12/306.
- [20] J.-P. Bourgoin, G.-G. Allogho, and A. Haché, “Thermal conduction in thin films measured by optical surface thermal lensing”, *J. Appl. Phys.*, vol. 108, no. 7, article no. 073520 (6 pages), Oct. 2010. DOI:10.1063/1.3490185.
- [21] W. Ma, T. Miao, Z. Xing, M. Kohno, and Y. Takata, “Comprehensive Study of Thermal Transport and Coherent Acoustic-Phonon Wave Propagation in Thin Metal Film-Substrate by Applying Picosecond Laser Pump-Probe Method”, *J. Phys. Chem. C*, vol. 119, no. 9, pp. 5152–5159, Feb. 2016. DOI: 10.1021/jp512735k.
- [22] J. S. Reparaz *et al.*, “A novel contactless technique for thermal field mapping and thermal conductivity determination: Two-Laser Raman Thermometry”, *Rev. Sci. Instrum.*, vol. 85, no. 3, article no. 034901 (5 pages), Mar. 2014. DOI: 10.1063/1.4867166.
- [23] Q. Y. Li *et al.*, “Optical absorptance measurement of an individual multiwall carbon nanotube using a T type thermal probe method”, *Rev. Sci. Instrum.*, vol. 84, no. 10, article no. 104905 (4 pages), Oct. 2013. DOI: 10.1063/1.4824494.

- [24] Q. Y. Li and X. Zhang, “T-type Raman spectroscopy method for determining laser absorption, thermal conductivity and air heat transfer coefficient of micro/nano fibers”, *Thermochim. Acta*, vol. 581, pp. 26-31, Apr. 2014. DOI: 10.1016/j.tca.2014.01.023.
- [25] Q. Y. Li, X. Zhang, and Y. D. Hu, “Laser flash Raman spectroscopy method for thermophysical characterization of 2D nanomaterials”, *Thermochim. Acta*, vol. 592, pp. 67-72, Aug. 2014. DOI:10.1016/j.tca.2014.08.011.
- [26] Q. Y. Li, W. G. Ma, and X. Zhang, “Laser flash Raman spectroscopy method for characterizing thermal diffusivity of supported 2D nanomaterials”, *Int. J. Heat Mass Tran.*, vol. 95, pp. 956-963, Apr. 2016. DOI:10.1016/j.ijheatmasstransfer.2015.12.065.
- [27] S. Xu, T. Wang, D. Hurley, Y. Yue, and X. Wang, “Development of time-domain differential Raman for transient thermal probing of materials”, *Opt. Express*, vol. 23, no. 8, pp. 10040-10056, Apr. 2015. DOI:10.1364/OE.23.010040.
- [28] T. Wang, S. Xu, D. H. Hurley, Y. Yue, and X. Wang, “Frequency-resolved Raman for transient thermal probing and thermal diffusivity measurement”, *Opt. Lett.*, vol. 41, no. 1, pp. 80-83, Jan. 2016. DOI:10.1364/OL.41.000080.
- [29] Q. Y. Li, *et al.*, “Measurement of thermal contact resistance between individual carbon fibers using a laser-flash Raman mapping method”, *Carbon*, vol. 141, pp. 92-98, Jan. 2019. DOI: 10.1016/j.carbon.2018.09.034.

- [30] Q. Y. Li, X. Zhang, and K. Takahashi, "Variable-spot-size laser-flash Raman method to measure in-plane and interfacial thermal properties of 2D van der Waals heterostructures" *Int. J. Heat Mass Tran.*, vol. 125, pp. 1230-1239, May 2018. DOI: 10.1016/j.ijheatmasstransfer.2018.05.011
- [31] Q. Y. Li, K. Takahashi, and X. Zhang, "Frequency-domain Raman method to measure thermal diffusivity of one-dimensional microfibers and nanowires" *Int. J. Heat Mass Tran.*, vol. 134, pp. 539-546, Jan. 2019. DOI: 10.1016/j.ijheatmasstransfer.2019.01.057
- [32] A. Fan, Y. Hu, W. Ma, H. Wang, and X. Zhang, "Dual-Wavelength Laser Flash Raman Spectroscopy Method for In-Situ Measurements of the Thermal Diffusivity: Principle and Experimental Verification", *J Therm. Sci.*, vol. 28, no. 2, pp.159-168, Mar. 2019. DOI: 10.1007/s11630-019-1084-x.
- [33] A. Fan, Y. Hu, H. Wang, W. Ma, and X. Zhang, "Dual-wavelength flash Raman mapping method for measuring thermal diffusivity of suspended 2D nanomaterials", *Int. J. Heat Mass Tran.*, vol. 143, article no. 118460 (9 pages), Nov. 2019. DOI:10.1016/j.ijheatmasstransfer.2019.118460.
- [34] Y. Zhang *et al.*, "Suspended 2D anisotropic materials thermal diffusivity measurements using dual-wavelength flash Raman mapping method", *Int. J. Heat Mass Tran.*, vol. 145, article no. 118795 (10 pages), Dec. 2019. DOI: 10.1016/j.ijheatmasstransfer.2019.118795.
- [35] Y. Hu, A. Fan, H. Wang, W. Ma, and X. Zhang, "Dual-wavelength flash Raman mapping method for measuring thermal diffusivity of the suspended nanowire", *Sci. China Technol. Sc.*,

vol. 63, no. 5 , pp. 748-754, May 2020. DOI:10.1007/s11431-019-9558-3.

LIST OF FIGURE CAPTIONS

- Figure 1 Schematic of the supported two-dimensional nanomaterial sample and the substrate.
- Figure 2 (a) Normalized temperature difference $f^{st}(r)/f^{st}(0)$ for various η_{sub}/λ_{sub} ;
(b) Temperature difference $f^{st}(r)$ for various λ_{sub}/g with a certain $\theta_{sub}^{st}(r,0)$.
- Figure 3 (a) Normalized temperature difference $f^{st}(r)/f^{st}(0)$ for various η_n/λ_n ;
(b) Temperature difference for $f^{st}(r)$ various λ_n/g with a certain $\theta_n^{st}(r)$.
- Figure 4 Normalized temperature rise curves of the supported sample for various α_n ($g/\lambda_n=3\times 10^4 \text{ m}^{-1}$, heating pulse width $t_h = 50 \text{ ns}$, temperature difference is assumed as 0.01 of the temperature rise of the corresponding suspended sample).
- Figure 5 (a) Normalized temperature distributions and (b) normalized sensitivities for various CC_{ste} .
- Figure 6 Normalized temperature variation curves at different positions with Fo changes $\pm 20\%$ (a) $CC_e = 0.001$, (b) $CC_e = 0.1$.
- Figure 7 System error of CC caused by simplifying assumption for various δT_{ste} and CC .
- Figure 8 System error of α_n caused by simplifying assumption for various δT and CC .
- Figure 9 System error of α_n caused by ignoring substrate temperature rise for various δT and CC .

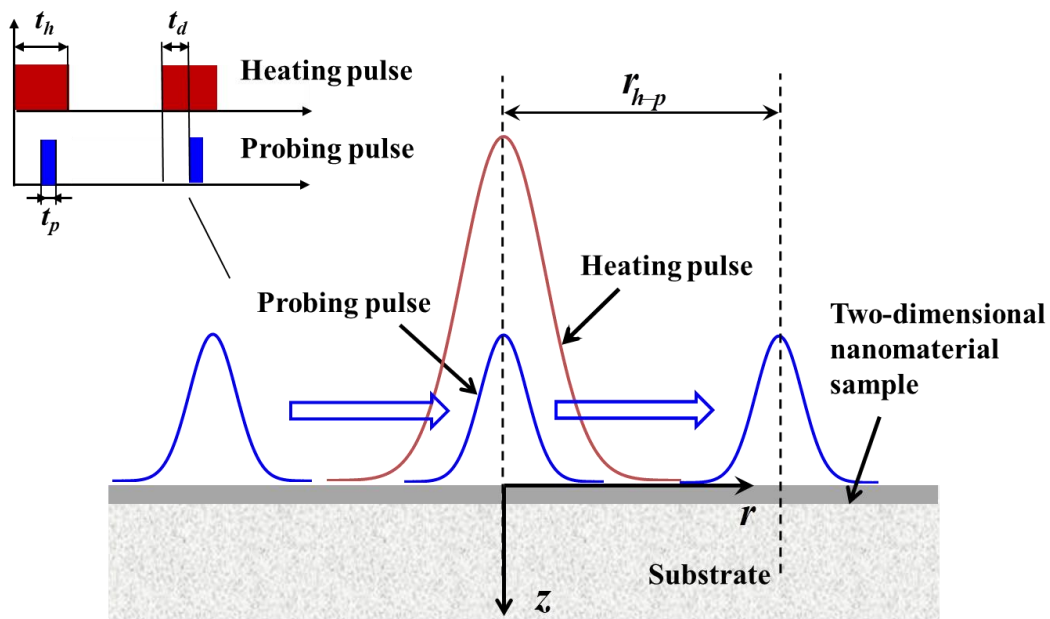
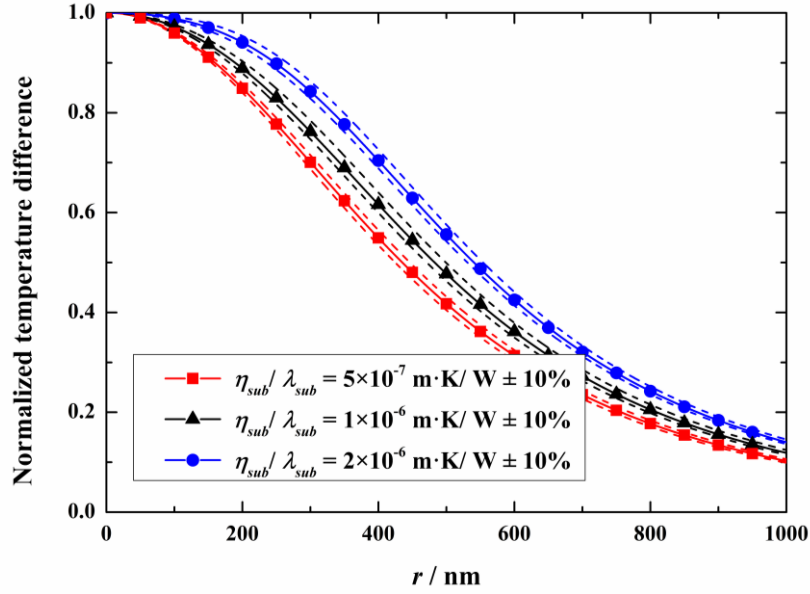
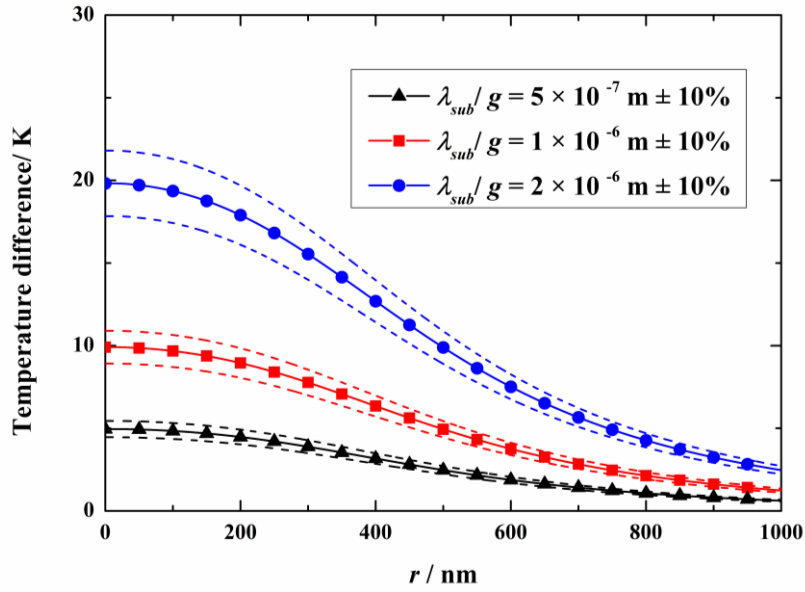


Figure 1. Schematic of the supported two-dimensional nanomaterial sample and the substrate.



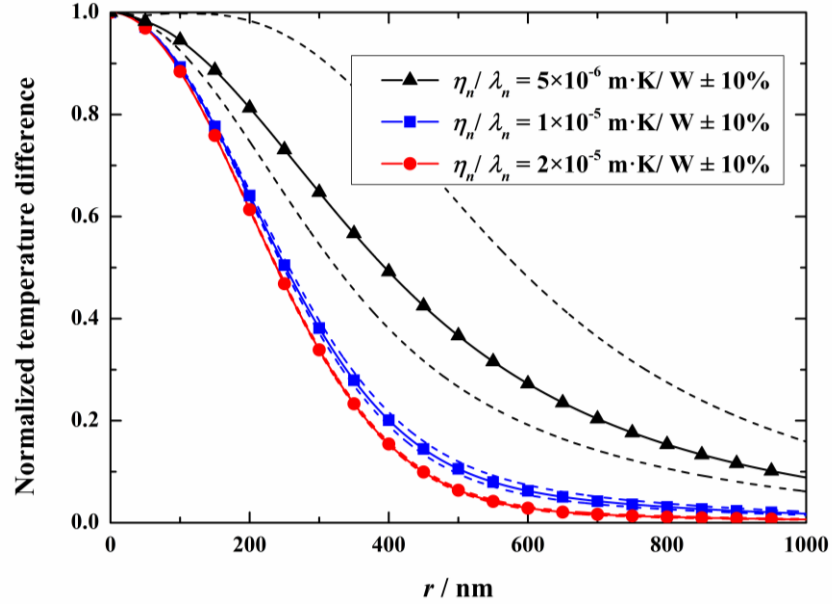
(a) Normalized temperature difference $f^{st}(r)/f^{st}(0)$ for various η_{sub}/λ_{sub}



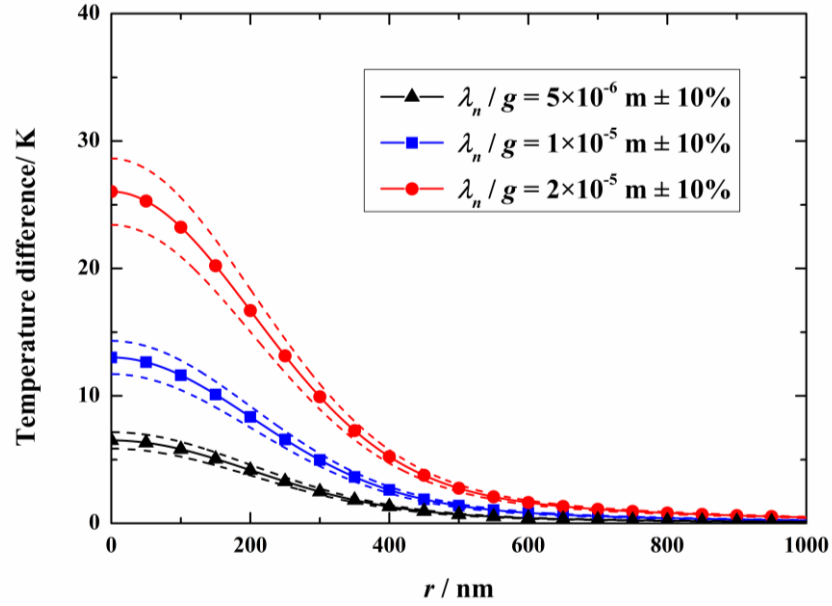
(b) Temperature difference $f^{st}(r)$ for various λ_{sub}/g with a certain $\theta_{sub}^{st}(r,0)$

Figure 2. (a) Normalized temperature difference $f^{st}(r)/f^{st}(0)$ for various η_{sub}/λ_{sub} ;

(b) Temperature difference $f^{st}(r)$ for various λ_{sub}/g with a certain $\theta_{sub}^{st}(r,0)$.



(a) Normalized temperature difference $f^{st}(r)/f^{st}(0)$ for various η_n/λ_n



(b) Temperature difference for $f^{st}(r)$ various λ_n/g with a certain $\theta_n^{st}(r)$

Figure 3. (a) Normalized temperature difference $f^{st}(r)/f^{st}(0)$ for various η_n/λ_n ;

(b) Temperature difference for $f^{st}(r)$ various λ_n/g with a certain $\theta_n^{st}(r)$.

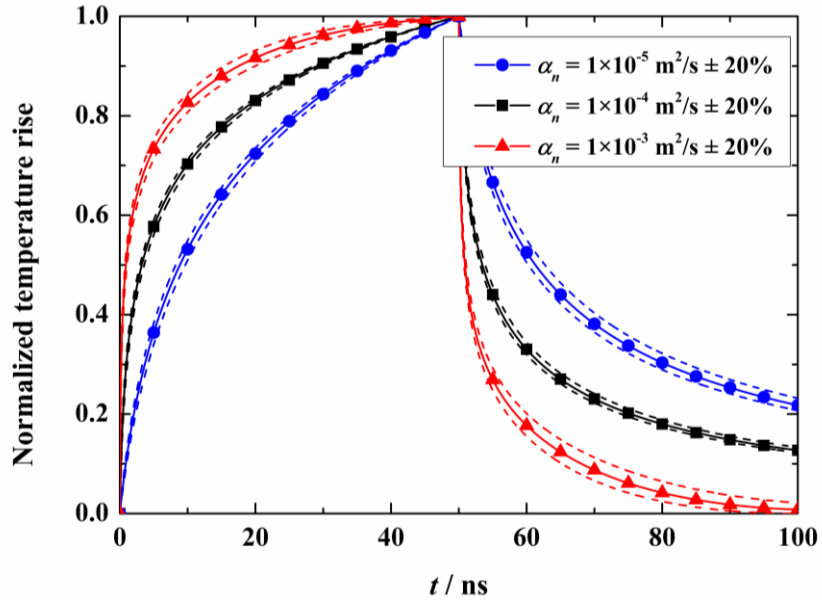
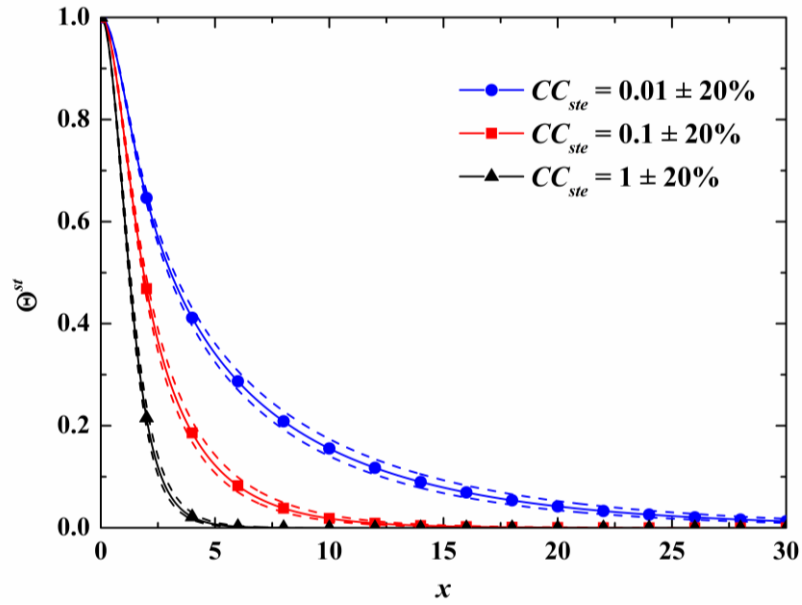
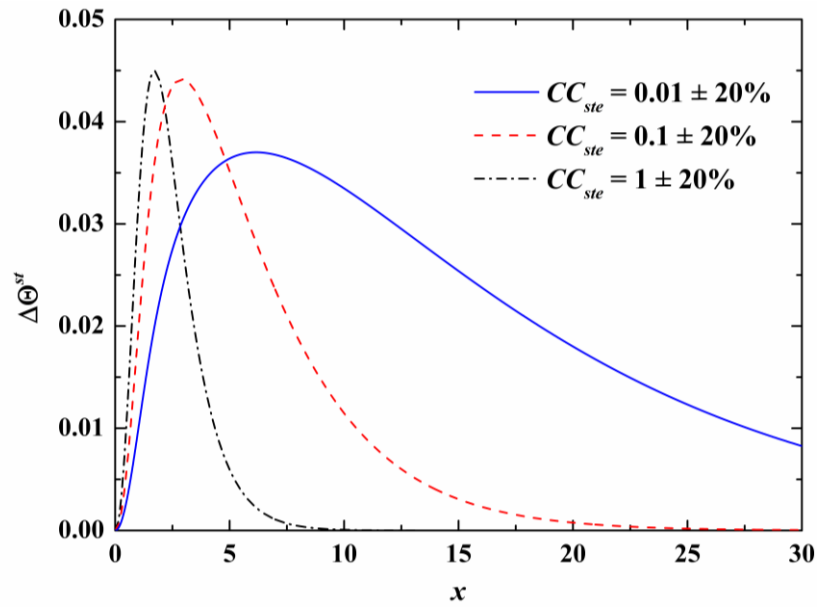


Figure 4. Normalized temperature rise curves of the supported sample for various α_n ($g/\lambda_n=3 \times 10^4 \text{ m}^{-1}$, heating pulse width $t_h = 50 \text{ ns}$, temperature difference is assumed as 0.01 of the temperature rise of the corresponding suspended sample).

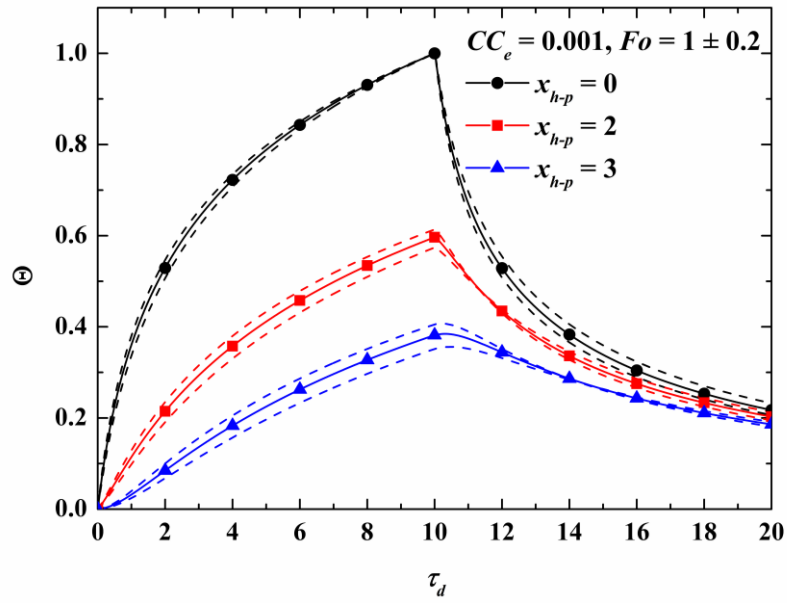


(a) Normalized temperature distributions for various CC_{ste}

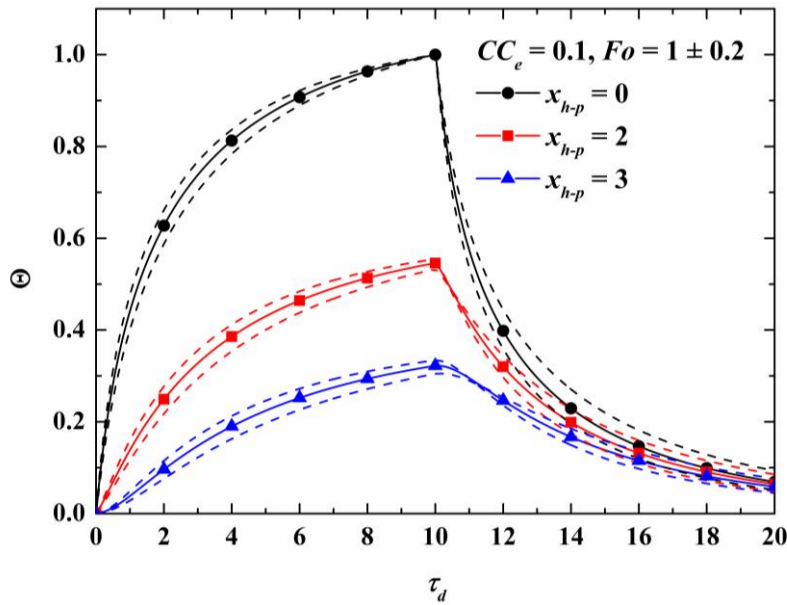


(b) normalized sensitivities for various CC_{ste}

Figure 5. (a) Normalized temperature distributions and (b) normalized sensitivities for various CC_{ste} .



(a) $CC_e = 0.001$



(b) $CC_e = 0.1$

Figure 6. Normalized temperature variation curves at different positions with Fo changes $\pm 20\%$

(a) $CC_e = 0.001$; (b) $CC_e = 0.1$.

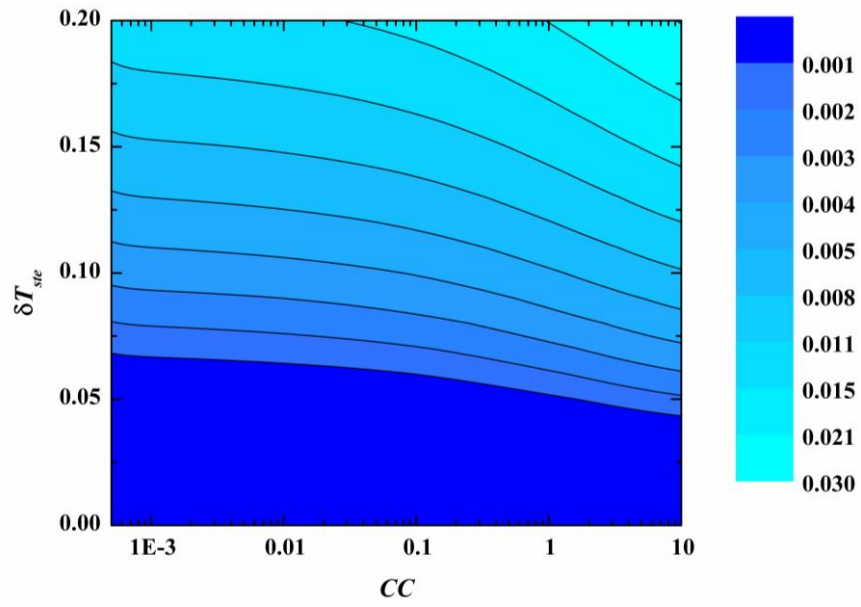


Figure 7. System error of CC caused by simplifying assumption for various δT_{ste} and CC .

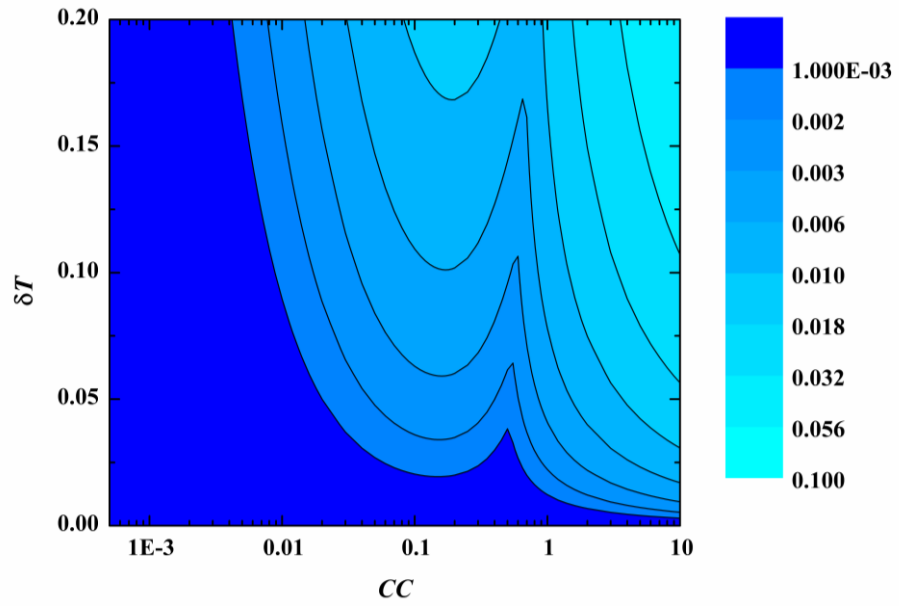


Figure 8. System error of α_n caused by simplifying assumption for various δT and CC .

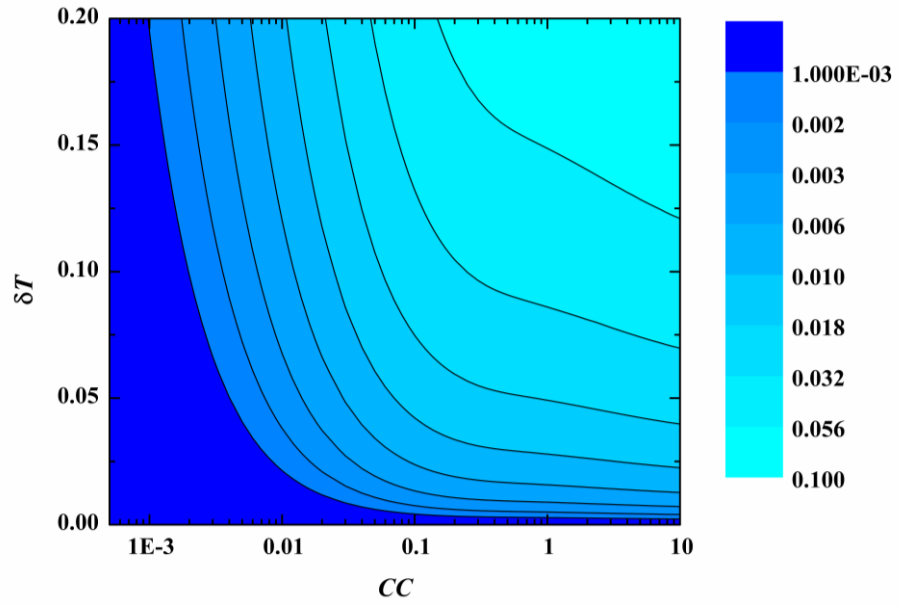


Figure 9. System error of α_n caused by ignoring substrate temperature rise for various δT and CC .

Notes on Contributors



Aoran Fan received the B.E. degree from Tsinghua University in 2015. She is a Ph.D. candidate of the Department of Engineering Mechanics at Tsinghua University, China. Her research interests focus on thermophysical properties measurement and interfacial effect at micro/nanoscale.



Haidong Wang received the B.E. (2006) and Ph.D. (2011) degrees from Tsinghua University. He is now an Associate Professor at Tsinghua University, China. His research interests include nanoscale heat transfer, low-dimensional materials, MEMS technology, and thermal functional devices.



Weigang Ma received the B.E. (2006) and Ph.D. (2012) degrees from Tsinghua University. He is an Associate Professor in the Department of Mechanical Engineering, Tsinghua University, China. His current interests mainly focus on micro/nanoscale transport and energy conversion.



Xing Zhang received the B.E. (1982) and M.E. (1985) degrees from Southeast University, and Ph.D. (1988) degree from Tsinghua University. He is a Professor in the Department of Engineering Mechanics, Tsinghua University, China. His current research interests include micro/nanoscale heat transfer, thermophysical properties of nanostructured materials, and efficient use of wind/solar/hydrogen energy.